Deciphering the atomic structure of a complex Sr/Ge (100) phase via scanning tunneling microscopy and first-principles calculations

Boris Lukanov, Kevin Garrity, Sohrab Ismail-Beigi, and Eric I. Altman

Phys. Rev. B **85**, 195316 — Published 15 May 2012

DOI: 10.1103/PhysRevB.85.195316

Deciphering the atomic structure of a complex Sr/Ge (100) phase via scanning tunneling microscopy and first principles calculations

Boris Lukanov,[1,2] Kevin Garrity,[2,3] Sohrab Ismail-Beigi,[2,3] and Eric I. Altman[2,4,*]

[1]*Department of Mechanical Engineering and Materials Science, Yale University, New Haven, CT 06520, USA*
[2]*Center for Research on Interface Structures and Phenomena (CRISP), Yale University, New Haven, CT 06520, USA*
[3]*Department of Applied Physics, Yale University, New Haven, CT 06520, USA*
[4]*Department of Chemical and Environmental Engineering, Yale University, New Haven, CT 06520, USA*

(Dated: May 2, 2012)

The details of a Sr-induced (3×4) reconstruction on Ge(100) were examined using scanning tunneling microscopy (STM) and density functional theory. At 1/6 ML of Sr, this reconstruction is similar to the 1/6 ML (3×2) Sr phase previously observed on Si. In contrast to Si, however, atomic-resolution images of the Sr-Ge phase exhibit more dramatic and unusual bias dependence in STM that could be explained with the help of first principles calculations of minimum energy structures. Simulated STM images are in excellent agreement with the experimental data and allow the (3×2) Sr-Si double dimer vacancy alloy model to be extended to the Ge surface through a more complex (3×4) arrangement of its building blocks. The difference between Si and Ge is interpreted in terms of the lower Ge-Ge binding energy and differences in the interatomic bond lengths.

PACS numbers: 68.35.bg, 68.37.Ef, 68.55.A-, 73.20.At

Technological and fundamental considerations have sparked interest in the growth of materials on the Ge(100) surface. The former centers on the importance of Si-Ge alloys and strained Ge to high speed microelectronics. The fundamental interest is motivated by the self-organization of metal atoms deposited onto Ge (100) into one-dimensional chains as narrow as one atom wide, the structure and properties of which have been intensely debated in the literature.[1–10] Curiously, depositing the same metals onto the chemically and structurally similar Si(100) surface does not cause analogous structures to form,[11,12] suggesting that subtle differences in the surface energetics of the two materials enable the Ge surface to promote the growth of 1-D structures.

In addition, the formation of submonolayer ordered alkaline earth layers on semiconductor surfaces has been an essential step in all successful oxide epitaxy on the technologically important (100) surfaces.[13,14] These high quality oxide films offer the promise of integrating ferroelectric, ferromagnetic, and superconducting functionalities with traditional semiconductor technology.[13] In order to improve understanding of the formation of interfaces between complex oxides and semiconductors, we have been studying the growth of alkaline earth layers on Si and Ge surfaces using a combination of electron and x-ray diffraction, first principles theory, and STM. While atomic-resolution STM studies of alkaline earths on Si have already emerged in the literature,[15,16] similar high resolution data for Ge(100) have been lacking.

Recently, we delineated the structural transitions that occur as Sr is deposited onto Ge(100) at elevated temperatures.[17] With increasing coverage, a series of phase transitions accompanied by substantial morphological restructuring was observed. This paper focuses on the atomic structure of the first ordered phase in the sequence: the (3×4) that saturates at 1/6 ML Sr. It will be shown that STM images of this surface depend dramatically on bias, making structural assignments based on experimental data alone challenging. Theoretical analysis of the energetics of candidate structures and comparison of simulated and experimental STM images, however, enabled assignment of the structure to a surface alloy phase. The building blocks for this structure are the same double dimer vacancy units we previously proposed for the (3×2)-Sr/Si(100)[18] and were subsequently studied by STM.[16] Staggering these blocks in a (3×4) arrangement, however, reduces the energy on Ge. The origin of this difference between Si and Ge will be interpreted in terms of the lower Ge-Ge binding energy and the tendency of Ge to favor structures that allow for a reduced Ge-Sr bond length.

Experiments were carried out using an ultra-high vacuum chamber equipped with a scanning tunneling microscope, quartz crystal deposition rate monitor, Ge and Sr evaporators, and the necessary sources and detectors for low energy electron diffraction and Auger electron spectroscopy.[17] Substrates were cut from undoped Ge wafers and were held at 675 K during Sr deposition, then quickly flashed to 900 K before imaging at room temperature. Electrochemically etched W tips were used for STM imaging. Constant current images were recorded at setpoint currents of 0.2 nA.

The Sr/Ge system was modeled using first-principles density functional theory (DFT) calculations with a plane wave basis set and ultrasoft pseudopotentials.[19–21] We use a slab geometry with 8-10 layers Ge and symmetric surfaces.[18] The generalized gradient approximation was used to model the exchange correlation function;[22] STM images were simulated using the Tersoff-Hamann method.[23,24]

The general features of (3×4) terraces are illustrated in the filled and empty state STM images in Fig. 1. The filled state image in Fig. 1(a) is populated by staggered oblong features surrounded by dark undulating lines that

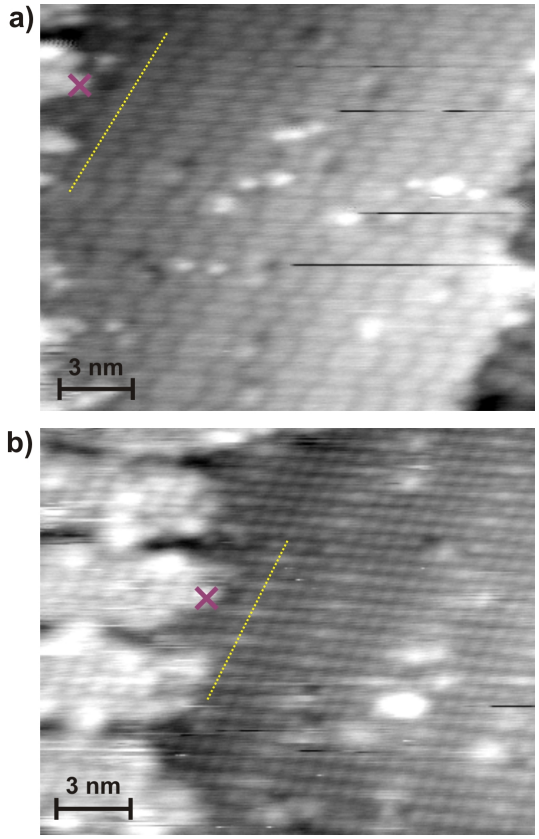

FIG. 1. (color online) a) Filled state (-2 V) and b) empty state (2 V) STM images of 1/6 ML Sr on Ge(100). The x indicates the same spot on the surface, while the dotted line highlights the same line of defects.

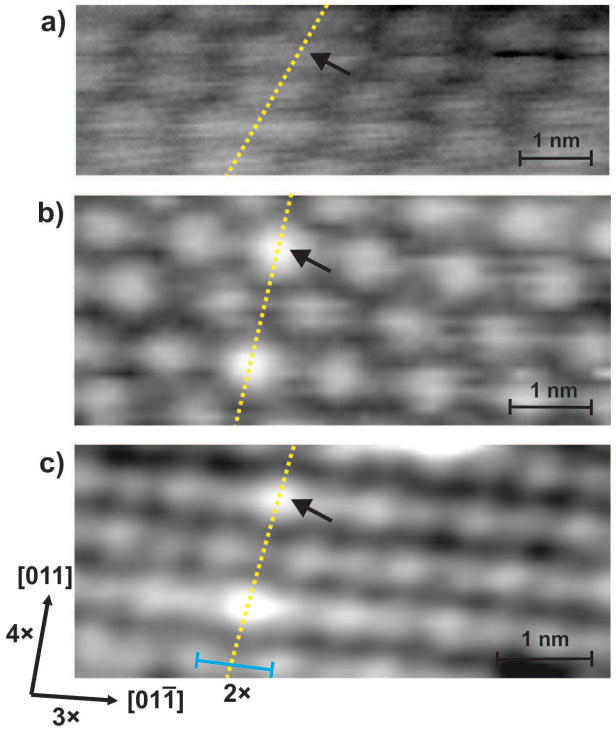

FIG. 2. (color online) (a) Filled state and (b-c) empty state close-up STM images of areas with 3×4 symmetry and a line of defects (dashed line). Arrows point to the same defect in all three images. Sample biases were -2 V (a), 1 V (b), 1.75 V (c).

run close to vertical in the image. The surface also exhibits point defects such as dark spots that resemble vacancies, as well as bright spots. Some of the oblong features appear as wider "dashes", the dotted line in Fig. 1(a) highlights a line of such defects. More interestingly, the empty state image recorded at 2 V in Fig. 1(b) appears completely different; here the surface is characterized by a rectangular grid of circular spots. The dotted line drawn at the same location on the surface in the two images shows that the line defects appear as rows of alternating brighter spots and missing spots in the empty state image.

The atomic scale details are better illustrated through the close-up images in Fig. 2 that show the (3×4) unit cells and a line defect at three biases. The filled-state image in Fig. 2(a) reveals oblong building blocks that form straight rows along the 3× [01$\bar{1}$] direction but are staggered along [011]. In (3×4) domains, the oblong units stagger in phase; i.e., adjacent building blocks move left and right together as the surface is traversed in the 4× direction. On opposite sides of the line defect the oblong building blocks are staggered out of phase, thus identifying the defect as an anti-phase domain boundary (APB). As a consequence of the regularly alternating long and short features along the APB, the distances between the building blocks on opposite sides of the boundary alternate.

While filled state images were relatively insensitive to bias, empty-state images exhibited strong variations with bias. At lower positive sample biases (≈ 1 V), the images revealed nearly centered rectangular patterns as illustrated in Fig. 2(b). A centered pattern is very puzzling for a surface with 3× symmetry, as it requires identical features to be situated at inequivalent sites. At these lower biases, the line defect appears as a row of slightly brighter spots. Consistent with the assignment of the line defects as APBs, the spots on either side of the APB are slightly displaced toward the row of brighter spots. As the bias was increased, additional bright spots appeared halfway between the spots seen at lower biases. As shown in Fig. 2(c), by 1.75 V these extra spots appeared at nearly the same height as the spots seen at lower biases. Interestingly, the extra spots are absent from APBs.

The complexity of the images and their strong dependence on bias make it difficult to determine the positions of the Ge and Sr atoms based on the experimental data alone. Therefore, the atomic-scale structure of the Sr-modified Ge surface was also studied using DFT. Similar to Sr on Si, if the Ge surface atoms are locked in the dimerized bare surface reconstruction, the lowest energy

TABLE I. Energies and characteristic distances for 1/6 ML Sr structures on Ge(100) and Si(100).

Substrate	Unit Cell	Vacancies(ML)	E_{bind}(eV/Sr)	Sr bond(Å)
Ge	Chain	0	3.47	
Ge	2×3	1/3	3.50	
Ge	3×2	2/3	3.53	3.29
Ge	3×4	2/3	3.54	3.25
Si	3×2	2/3	3.90	3.26
Si	3×4	2/3	3.89	3.23

1/6 ML structure has the Sr in the same binding site as an isolated Sr atom, i.e. in the trough between four Ge dimers.[18,25] Sr fills these sites in disordered chain-like structures with a binding energy of 3.47 eV/Sr (see Table I).[18,25,26] We have shown, however, that formation of the (3×4) structure is accompanied by changes in the step structure indicative of growth due to Sr incorporation into the surface and Ge ejection from the original terraces[17] and is consistent with metal-induced restructuring of Ge surfaces seen at temperatures as low as 475 K.[4–6] Therefore, we must also consider mixed Sr-Ge surfaces.

Based on our prior results for Sr on Si, two structural motifs in which Sr replaces surface Ge were considered: 1) a (2×3) single dimer vacancy structure in which each Sr replaces one Ge dimer; and 2) a (3×2) double dimer vacancy structure in which each Sr replaces two Ge dimers.[18,27] Both structures are more stable than the chain-like structure considered above, and, similar to Si, the second is more stable as indicated in Table I. As shown in the side view of the more stable structure in Fig. 3(a), its building block can be pictured as the double-dimer vacancy defect often seen on contaminated Si and Ge(100) surfaces,[4,28,29] with Sr filling one of the two second layer four-fold hollows exposed by the missing dimers. In contrast to Si, it is slightly more favorable (by only 0.01 eV/Sr) to arrange these building blocks on Ge(100) by staggering them on adjacent dimer rows as pictured in Fig. 3(b). The result is the observed (3×4) periodicity.

The unusual bonding pattern of the (3×4) model explains the appearance and strong bias dependence of the STM images. In this structure, Sr donates its two valence electrons to two of the low-lying half-filled dangling bond states on the surrounding Ge atoms. More surprisingly, the top-layer Ge dimer, which is distorted into an unusual planar sp^2 bonding geometry rather than the typical Ge sp^3 tetrahedral configuration, also donates two electrons from its high-energy dangling p_z-like states to the lower energy dangling bond states of the adjacent Ge atoms bonded to Sr. This can be seen in the partial density of states shown in Fig. 3(c), which shows filled dangling bond states just below the Fermi level (E_F) centered on the second layer Ge atoms, and empty states from the outermost Ge dimer just above E_F. The net result of this electron transfer is that the highest energy occupied states are the four passivated dangling bonds surrounding each Sr, and that the lowest energy unoccupied states are not due to Sr, but rather the dangling p_z-like states on the outermost Ge dimer.

The bonding outlined above counter-intuitively suggests that although Sr donates its valence electrons to Ge as expected, the highest density of filled states near E_F surround the Sr atoms, while the first unoccupied states encountered above E_F are surprisingly centered on the outermost Ge dimers. This results in the simulated STM images in Fig. 3(d-g) which are in excellent agreement with the experimental data. Below E_F, the simulated images all appeared similar to Fig. 3(d) with broad maxima that extend over the Sr atom and the four neighboring Ge atoms; these maxima are associated with the passivated dangling bond states and are relatively insensitive to bias. Although some of the finer details are not resolved in the experiment, the staggered pattern strongly resembles the experimental images in Figs. 1(a) and 2(a). In accord with experimental observations, simulations above E_F revealed a strong bias dependence. At the lowest positive bias (Fig. 3(e)), the calculations indicate that the images should be dominated by the p_z-like states of the outermost Ge dimers. As the bias is increased, the tunneling probability to empty s and d orbitals above the Sr atoms increases, accounting for the additional features seen in Fig. 3(f). Interestingly, as features associated with the Sr atoms become visible, the brightest spots form more of a centered rectangular pattern as seen experimentally. At high positive biases (Fig. 3(g)), the intensity of the spots due to Sr and the raised dimers are essentially equal, completing the experimentally observed trend. It should be noted that theory suggests that the Sr atoms should appear in empty state images at much lower biases than those seen experimentally. This is due to well-known difficulties in predicting bandgaps with DFT, thus the accurate prediction of the trend is more significant than an absolute comparison of the biases.

Theory also provided valuable insights into the APBs seen in Figs. 1 and 2. We find that the APBs can be constructed as a mixture of a c(8×4) structure with the (3×4) structure at 1/6 ML. The APB is characterized by two new structural motifs that alternate along the [011] direction as pictured in Fig. 4(a): a top-layer Ge dimer (light blue) with two neighboring Sr atoms (yellow) on both sides; and a Sr atom with top-layer Ge dimers on either side. As for the (3×4) surface, filled state images are dominated by the passivating bonds surrounding the Sr atoms leading to elongated features when two Sr atoms neighbor a Ge dimer and shortened features when two Ge dimers neighbor a Sr atom; this is shown schematically in Fig. 4(b). As in Fig. 2, the building blocks stagger out of phase on opposite sides of the APB. Meanwhile, the p_z-like dangling bond states of the Ge dimers with two neighboring Sr atoms are pushed downwards towards E_F making these features appear bright in empty state images recorded at low biases (Fig. 4(c)). In con-

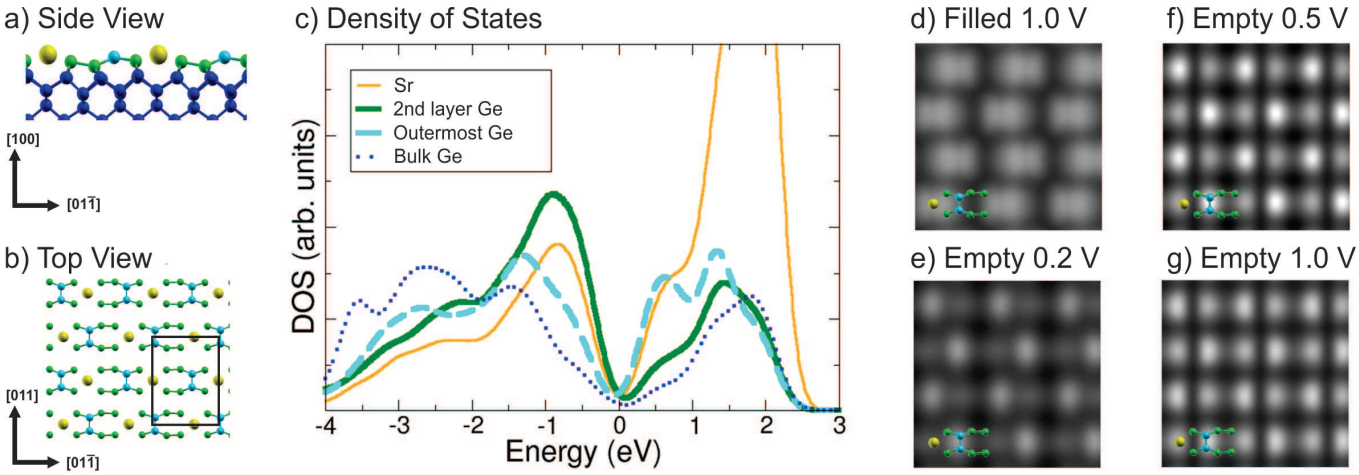

FIG. 3. (color online) a) Top view and b) side view of the 3×4 structure: Sr-large yellow, outermost Ge dimers-cyan, exposed surface Ge-green, and bulk Ge-dark blue. c) Partial density of states at different sites. d)-g) Simulated filled (d) and empty state (e)-(g) STM images.

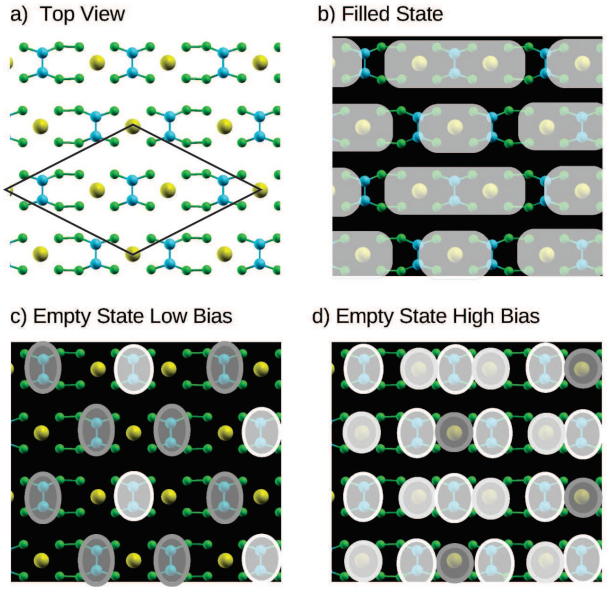

FIG. 4. (color online) Structure (a) and schematic STM images (b)-(d) of 3/16 ML Sr c(8×4) phase. The shaded areas highlight features predicted to appear in STM images, with whiter shading highlighting brighter features. Color scheme same as in Fig. 3

trast, the unoccupied s and d states of the Sr atoms with two neighboring Ge dimers shift towards higher energy making these features appear dim at positive biases (Fig. 4(d)). The Sr coverage in the local c(8×4) domains at the APBs is 3/16 ML compared to 1/6 ML in the (3×4) structure. Thus increasing the APB density can provide a mechanism to smoothly increase the Sr coverage from 1/6 to 3/16 ML.

As evident from Table I, our calculations suggest that the energy differences between the (3×2) and (3×4) Sr structures on Ge and Si are very small. Yet, experimentally there is a clear preference for the (3×4) reconstruction on Ge and the (3×2) on Si. Comparison of the Sr bond to the adjacent non-dimerized Ge for these two phases in Table I indicates that the (3×4) configuration leads to shorter bonds. The shorter Sr bonds, however, are accompanied by a greater distortion of the Ge-Ge (or Si-Si) bonds in the (3×4) phase which is evident in Fig. 3(a,b). These differences between the two phases may explain why the (3×4) phase is observed on Ge but not Si. First, the weaker Ge-Ge bonds, as evidenced by Ge's lower heat of sublimation (3.8 eV compared to 4.7 eV for Si), and Ge's lesser tendency towards sp^3 bonding, allows greater freedom to distort Ge-Ge bonds. Second, the larger Ge lattice constant provides a greater driving force to reduce Sr bond lengths by distorting substrate bonds. This argument is bolstered by the structures of bulk $SrSi_2$ and $SrGe_2$ alloys. The Ge-Sr and Si-Sr bond lengths are very similar in the two materials but in the Si compound the Si-Si bond lengths are almost identical to pure Si, while the Ge-Ge bond lengths are expanded compared to pure Ge.[30–32]

The alloy structures discussed in this paper provide further evidence that semiconductor surfaces are not static substrates for oxide growth, and that growth conditions must be carefully controlled to achieve the desired interface. The ability of the substrates to reconstruct in a variety of bonding geometries may prove useful in creating various interface structures on different substrates, or on the same materials under different conditions.

This project was supported by the National Science Foundation through the Yale Materials Research Science and Engineering Center (Grant No. MRSEC DMR-1119826).

* eric.altman@yale.edu

[1] O. Gurlu, O. A. O. Adam, H. J. W. Zandvliet, and B. Poelsema, App. Phys. Lett. **83**, 4610 (2003).
[2] M. Fischer, A. van Houselt, D. Kockmann, B. Poelsema, and H. J. W. Zandvliet, Phys. Rev. B **76**, 245429 (2007).
[3] A. A. Stekolnikov, F. Bechstedt, M. Wisniewski, J. Schäfer, and R. Claessen, Phys. Rev. Lett. **100**, 196101 (2008).
[4] J. Wang, M. Li, and E. I. Altman, Phys. Rev. B **70**, 233312 (2004).
[5] J. Wang, M. Li, and E. I. Altman, Surface Science **596**, 126 (2005).
[6] A. van Houselt, M. Fischer, B. Poelsema, and H. J. W. Zandvliet, Phys. Rev. B **78**, 233410 (2008).
[7] R. Niikura, K. Nakatsuji, and F. Komori, Phys. Rev. B **83**, 035311 (2011).
[8] J. Schäfer, C. Blumenstein, S. Meyer, M. Wisniewski, and R. Claessen, Phys. Rev. Lett. **101**, 236802 (2008).
[9] A. van Houselt, D. Kockmann, T. F. Mocking, B. Poelsema, , and H. J. W. Zandvliet, Phys. Rev. Lett. **103**, 209701 (2009).
[10] D. E. P. Vanpoucke and G. Brocks, Phys. Rev. B **81**, 085410 (2010).
[11] M. Kageshima, Y. Torii, Y. Tano, O. Takeuchi, and A. Kawazu, Surf. Sci. **472**, 51 (2001).
[12] H. Itoh, S. Narui, A. Sayama, and T. Ichinokawa, Phys. Rev. B **45**, 11136 (1992).
[13] J. Reiner, A. Kolpak, Y. Segal, K. Garrity, S. Ismail-Beigi, C. Ahn, and F. Walker, Adv. Mat. **22**, 2919 (2010).
[14] R. A. McKee, F. J. Walker, and M. F. Chisholm, Phys. Rev. Lett. **81**, 3014 (1998).
[15] W. Du, B. Wang, L. Xu, Z. Hu, X. Cui, B. C. Pan, J. Yang, and J. G. Hou, J. Chem. Phys. **129**, 164707 (2008).
[16] J. He, G. Zhang, J. Guo, Q. Guo, and K. Wu, J. Appl. Phys. **109**, 083522 (2011).
[17] B. R. Lukanov, J. W. Reiner, F. J. Walker, C. H. Ahn, and E. I. Altman, Phys. Rev. B **84**, 075330 (2011).
[18] K. Garrity and S. Ismail-Beigi, Phys. Rev. B. **80**, 085306 (2009).
[19] P. Hohenberg and W. Kohn, Phys. Rev. **136**, B864 (1964).
[20] W. Kohn and L. Sham, Phys. Rev. **140**, A1133 (1965).
[21] D. Vanderbilt, Phys. Rev. B **41**, 7892 (1990).
[22] J. P. Perdew, K. Burke, and M. Ernzerhof, Phys. Rev. Lett. **77**, 3865 (1996).
[23] J. Tersoff and D. R. Hamann, Phys. Rev. Lett. **50**, 1998 (1983).
[24] J. Tersoff and D. R. Hamann, Phys.Rev. B **31**, 805 (1985).
[25] C. R. Ashman, C. J. Först, K. Schwarz, and P. E. Blöchl, Phys. Rev. B **69**, 075309 (2004).
[26] K. F. Garrity, M.-R. Padmore, Y. Segal, J. Reiner, F. Walker, C. Ahn, and S. Ismail-Beigi, Surface Science **604**, 857 (2010).
[27] J. W. Reiner, K. F. Garrity, F. J. Walker, S. Ismail-Beigi, and C. H. Ahn, Phys. Rev. Lett. **101**, 105503 (2008).
[28] V. A. Ukraintsev and J. T. Yates, Surf. Sci. **346**, 31 (1996).
[29] C. S. Chang, Y. M. Huang, C. C. Chen, and T. T. Tsong, Surf. Sci. **367** (1996).
[30] J. Evers and A. Weiss, Mat. Res. Bull. **9**, 549 (1974).
[31] Y. Imai and A. Watanabe, Intermetallics **14**, 666 (2006).
[32] A. Palenzona and M. Pani, J. Alloy. Compd. **402**, 136 (2005).